LETTER

Single photon emission dynamics of InP-InGaP quantum dots under p-shell excitation

To cite this article: A. K. Nowak *et al* 2014 *EPL* **108** 17002

A Letters Journal Exploring the Frontiers of Physics

October 2014

EPL, **108** (2014) 17002 www.epljournal.org
doi: 10.1209/0295-5075/108/17002

Single photon emission dynamics of InP-InGaP quantum dots under p-shell excitation

A. K. Nowak[1,2], M. D. Martín[1,3], H. P. van der Meulen[1,3], J. M. Ripalda[4], L. González[4], Y. González[4], L. Viña[1,3,5] and J. M. Calleja[1,3,5]

[1] *Departamento de Física de Materiales, Universidad Autónoma de Madrid, Unidad Asociada CSIC-SEMICUAM E-28049 Madrid, Spain*
[2] *Laboratoire de Photonique et de Nanostructures, CNRS, UPR20 - Route de Nozay, 91460 Marcoussis, France*
[3] *Instituto de Ciencia de Materiales "Nicolás Cabrera", Universidad Autónoma de Madrid - Madrid 28049, Spain*
[4] *Instituto de Microelectrónica de Madrid, Centro Nacional de Microelectrónica, CSIC - Isaac Newton 8, Tres Cantos, E-28760 Madrid, Spain*
[5] *Condensed Matter Physics Center (IFIMAC), Universidad Autónoma de Madrid - Madrid 28049, Spain*

received 8 May 2014; accepted in final form 11 September 2014
published online 24 September 2014

PACS 78.55.Et – II-VI semiconductors
PACS 85.35.Be – Quantum well devices (quantum dots, quantum wires, etc.)
PACS 42.50.Ar – Photon statistics and coherence theory

Abstract – Single photon emitters based on InP/GaInP quantum dots have been studied under *p*-shell excitation by time-resolved photoluminescence and photon correlation spectroscopy. By tuning the excitation energy in resonance with quantum dot excited states, we observe a marked decrease of the antibunching time as a result of the increased excitation rate for decreasing energy detuning. A similar behavior is observed by increasing the pump power. The spectral dependence of the antibunching rate follows the energy profile of the excited state, as measured by photoluminescence excitation.

The efficient emission of single photons has been searched in the last decade because of the rapidly developing field of quantum information science and technology. Quantum computation and cryptography require triggered single photon or entangled photon pair sources with well-established spectral and temporal characteristics. This can be achieved with sources of strongly correlated photons, like single atoms or ions [1,2] molecules [3,4], defect centers in diamond [5,6] or semiconductor quantum dots (QDs) [7]. Among them, QDs are technologically attractive for their design flexibility and integration capability in monolithic optoelectronic devices. However, the reliability of single photon emitters (SPE) based on single semiconductor QDs is strongly affected by fast decoherence due to coupling to phonons [8], as well as by the presence of background photons or multiphoton emission. The dynamics of the optical creation and recombination of excitons in a single QD is at the basis of its behavior as a SPE. Essential SPE characteristics, such as the recharging time, repetition rate or the appearance of bunching depend strongly on the excitation conditions (energy, intensity and time structure). In particular, excitation at energies above the QD potential barriers results in long relaxation processes and increased probability of QD charging. These effects are largely reduced under intra-dot excitation at the QD, *i.e.* upon resonant excitation at the confined QD states. Single photon emission in InAs QDs under pulsed excitation resonant with both *p*-states [9] and *s*-states [10] of a QD have been reported. Intra-dot excitation should also increase the quantum efficiency of the SPE [11,12]. Corresponding studies in InP QDs are comparatively scarce [13–18] in spite of the fact that they emit at higher energies, where the available single photon detectors are more efficient.

In this work we study the influence of the *p*-shell excitation conditions on the dynamics of the QD population, which determines SPE characteristics. We present the first evidence that the antibunching rate dependence on excitation energy exactly follows the spectral excitation profile of the *p*-shell. This implies that tuning the excitation energy inside the *p*-shell absorption peak allows to vary continuously the maximum repetition rate of a single photon emitter by a factor of five, at constant excitation power.

The detuning of the excitation energy with respect to the p-shell peak maximum controls the QD excitation rate in a similar way as the excitation power does. At low excitation powers, as well as at large detunings, one recovers an antibunching rate value coincident with the exciton decay rate, as measured by time-resolved spectroscopy. The memory effect [19,20] associated to long-time delays is also discussed.

The InP/GaInP QD samples were grown by molecular-beam epitaxy on GaAs (001) substrates. Details of the growth procedure can be found in ref. [14]. The QD density is approximately $3 \times 10^9\,\mathrm{cm}^{-2}$, as estimated by atomic force microscopy. The average diameter and height of the QDs before capping were 35 nm and 6 nm, respectively. However, the QDs selected for this work are those emitting at the high energy tail (1.84–1.87 eV) of the ensemble photoluminescence (PL) distribution. For this spectral range one observes isolated PL peaks corresponding to the emission of the smallest QDs. From their emission energies we estimate their height to be between 1 and 2 nm [13,14]. The high emission energy of these QDs prevents charge transfer from the neighboring dots and allows the observation of single QDs without the need of masks or mesas. The PL spectra of single QDs were taken through a 100× microscope objective (1 μm spot diameter) under variable excitation energy in the range between 1.875 eV and 1.960 eV using a continuous wave (cw) DCM (4-dicyanomethylene-2-6-p-dimethylaminostyryl-4H-pyran) dye laser. The detection was done by a double-grating spectrometer with a 0.85 m focal length, and a charged coupled device detector. PL excitation (PLE) measurements were performed using a computer controlled feedback system to synchronize the dye laser and a prism monochromator to eliminate the dye background emission. Single photon correlation (SPC) measurements were done with a Hanbury-Brown and Twiss (HBT) interferometer [21] located at one of the exits of a 0.75 m focal length single-grating spectrometer. Two avalanche photodiodes with 65% efficiency at the QD emission energy (1.86 eV) were used for coincidence detection. The HBT instrumental response time (τ_i = 0.5 ns) was measured using a pulsed Ti-sapphire laser (see below). The count rates at the detectors varied from 1.3×10^4 counts/s to 8×10^4 counts/s depending on the excitation power (P_e) and the excitation energy (E_e). Time-resolved photoluminescence (TRPL) measurements were performed in a micro-PL set-up. Excitation was performed using 2 ps pulses (82 MHz repetition rate) obtained from the second harmonic generated from a picosecond optical parametric oscillator (OPO) pumped with a Ti-sapphire laser. The excitation energy was 1.931 eV with an average power comparable to those used with cw excitation. The collection was done by a single-grating (0.5 m focal length) spectrometer combined with a streak camera whose instrumental response time was 10 ps. All the measurements were performed at temperatures below 15 K in a continuous flow He cryostat.

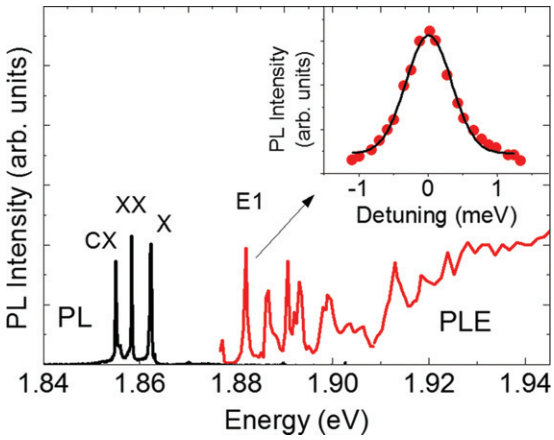

Fig. 1: (Color online) Micro-PL spectra (black line) of a typical single QD under excitation above the WL, and micro-PLE (red line) of the exciton (X) for 250 nW excitation power. The PL spectrum shows the single neutral (X) and charged (CX) exciton and the neutral biexciton (XX). The inset shows the E_1 transition at 1.882 eV in an enlarged scale (red symbols) and its Gaussian fit (black line).

The micro-PL and micro-PLE spectra of a typical single QD are plotted in fig. 1. Three emission lines corresponding to the neutral exciton (X), neutral biexciton (XX) and charged exciton (CX) are observed. The line assignment was performed by their intensity dependence on excitation power and by their linear polarization properties, as reported in ref. [14]. The micro-PLE spectrum of the X line displays several sharp peaks at energies between 20 meV and 40 meV above the detection energy. These lines correspond to absorption transitions involving QD excited states. The PLE peaks can be either pure electronic transitions between p-shell states or phonon-assisted absorption processes. The appearance of numerous PLE lines in a small, single QD is due to the presence of additional carriers in the excited states, which produce a rich manifold due to their Coulomb interactions [22]. The inset shows an enlarged view of the PLE data around the E_1 peak (red symbols) as a function of the excitation detuning ($\delta = E_e - E_1$) with respect to the E_1 energy. The data are well fitted by a Gaussian (black line) with a full width at half maximum of 0.77 ± 0.02 meV.

TRPL measurements done for excitation at 1.931 eV, (*i.e.* below the wetting layer) are shown in fig. 2. The time evolution of the X and XX emission intensities is shown in fig. 2(a). The experimental decays are fitted by a simple model [23] considering single exponentials for the population and depopulation of the X state with rates $1/\tau_P$ and $1/\tau_X$, respectively:

$$n_X(t) = C_X(e^{-t/\tau_X} - e^{-t/\tau_P}) \qquad (1)$$

and similarly for the XX state. The population channel for the exciton includes carrier relaxation from excited states of the QD and biexciton recombination, whereas the biexciton state is populated only by carrier relaxation. The excellent fits of eq. (1) to the experimental data (solid

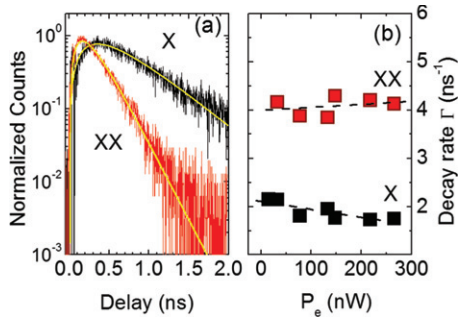

Fig. 2: (Color online) Time-resolved PL results: (a) X and XX PL time-evolution traces, together with fits (thick lines) with eq. (1). (b) Dependence of Γ_X (red squares) and Γ_{XX} (black squares) on excitation power measured at 12 K. The lines are linear fits to the experimental data.

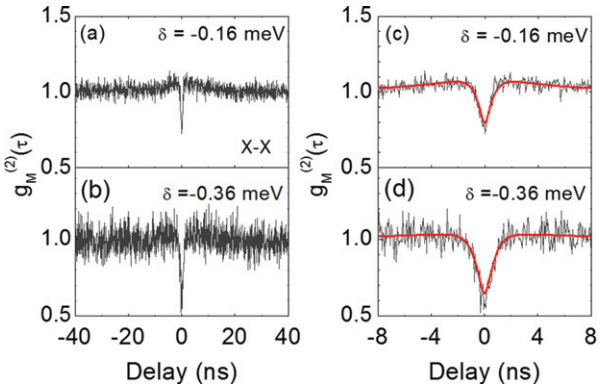

Fig. 3: (Color online) $g_M^{(2)}(\tau)$ for X measured for 230 nW for different values of the excitation detuning, δ, from the E_1 excited state: (a) and (c) $\delta = -0.16$ meV, (b) and (d) $\delta = -0.36$ meV. The solid lines are fits to the convolution of eqs. (2) and (3).

lines in fig. 2(a)) indicate that the exciton and biexciton populations decrease with a single decay time each. The role of dark to bright exciton transitions by spin-flip is known to play a role in InAs QDs leading to biexponential decays at times larger than 3–4 ns [24]. In our case the spin-flip time should be even larger, as the dark-bright energy splitting in small InP dots is of several meV [13,14], *i.e.* one order of magnitude larger than in InAs dots. This explains why dark excitons do not lead to bi-exponential decays in our case, at least in the time delay range studied. Besides, the exciton decay rate may contain one or several recombination channels (including spin-flip contributions). This fact is irrelevant for the analysis of the antibunching time (see below), provided that there is a single decay rate.

The decay rates extracted from the previous fit are shown in fig. 2(b) as a function of the time averaged excitation power P_e. One observes that Γ_{XX} is nearly power independent, while Γ_X (which is roughly one half of Γ_{XX}) shows a very weak decrease with increasing excitation power. The straight lines are fits to the experimental data. This is the expected trend for the exciton dynamics in a QD [23,25]. The radiative recombination from the XX state is allowed only into the bright X. Thus, any change in the probability of the XX occupation has a direct influence on the X population evolution. At high excitation power the QD in the X state captures a second electron-hole pair (e-h) before the first one can recombine radiatively. This QD *refilling* process is evident from the slower rise of the X intensity seen in fig. 2(a). In the low excitation-power limit the decay rates of X and XX tend to 2.1 ns^{-1} and 4.0 ns^{-1}, respectively. The fact that $\Gamma_{XX} \approx 2\Gamma_X$ over the whole excitation range indicates strong confinement (*i.e.* the exciton Coulomb interaction is small compared to the confinement energy) [26]. This is not surprising as we are dealing with the smaller dots of the QD distribution, where confinement is strongest. In this case the ratio $\Gamma_{XX}/\Gamma_X \approx 2$ simply reflects the double number of possible recombination channels of the biexciton compared to those of the exciton.

The SPE dynamics of the QD single photon emission under intra-dot excitation was studied in a second-order correlation experiment. The measurements were performed exciting at energies around the state E_1 in fig. 1. The X auto-correlation function $g^{(2)}(\tau)$ was measured under different values of the excitation power and detuning with respect to E_1. Plots of the *measured* function $g_M^{(2)}(\tau)$ at 230 nW excitation power for δ values of -0.16 and -0.36 meV are shown in figs. 3(a) and (b), respectively. This power is lower than the saturation value (around 300 nW) of the exciton intensity. A clear antibunching dip is observed at zero delay evidencing SPE, as well as bunching at a longer time scale. The same plots are shown in figs. 3(c) and (d) in an expanded delay scale together with the plots used to extract the relevant parameters, as shown next.

The experimental correlation curves $g_M^{(2)}(\tau)$ plotted in fig. 3 are the result of convoluting the *true* correlation function $g^{(2)}(\tau)$, given by [27]

$$g^{(2)}(\tau) = 1 - \beta e^{-|\tau|/\tau_R} + \alpha e^{-|\tau|/\tau_B} \qquad (2)$$

with the instrumental response function [28]

$$f_{IRF}(\tau) \sim e^{-|\tau|/\tau_i}. \qquad (3)$$

The parameters α and β ($\beta \leq \alpha + 1$) in eq. (2) represent the bunching and antibunching amplitudes, respectively. τ_R is the antibunching time, *i.e.* the time needed to produce a new (e-h) within the QD after the photon emission by a previous confined e-h pair. The bunching time τ_B represents the probability of multiphoton emission for delays $|\tau| > 0$. Both antibunching and bunching times (or the corresponding rates $\Gamma_R = \tau_R^{-1}$ and $\Gamma_B = \tau_B^{-1}$) as well as $g^{(2)}(0)$ are found by fitting the convolution of eqs. (2) and (3) to $g_M^{(2)}(\tau)$. The resulting values for $\delta = -0.16$ and $\delta = -0.36$ meV are given in table 1.

The most relevant result in table 1 is the decrease of the antibunching time for decreasing detuning. In both cases

Table 1: Parameters obtained from the fit of figs. 3(c) and (d), with eqs. (2) and (3).

δ (meV)	τ_R (ns)	τ_B (ns)	β	α
-0.16	0.20 ± 0.02	6 ± 1	1.10 ± 0.05	0.11 ± 0.05
-0.36	0.33 ± 0.03	20 ± 10	1.06 ± 0.05	0.06 ± 0.05

we obtain $g^{(2)}(0) = 1 - \beta + \alpha < 0.2$, which is indicative of true single photon emission. These low $g^{(2)}(0)$ values are essentialy insensitive to excitation power. Indeed we find similar values, within the experimental error, for the excitation powers (230 and 470 nW) used in fig. 4. This is due to the low photon background of our samples [14], being further reduced under intra-dot excitation. In fact, the $g^{(2)}(0)$ data under non-resonant excitation (< 0.25) [14], are only slightly worse, again due to the low photon background.

In the absence of carrier capture by neighboring QDs or defects, the antibunching rate is given by the sum of the QD pump rate (γ) and the exciton decay rate [7,29]

$$\Gamma_R = \gamma + \Gamma_X. \tag{4}$$

The increase of γ by increasing the excitation power produces the well-known narrowing of the antibunching dip observed at high P_e [7]. As the pump rate is proportional to both the excitation power and the absorption coefficient, γ can be also increased by resonant excitation at QD excited states, while keeping P_e constant. To show this equivalence we have performed measurements of Γ_R for excitation at resonance with the excited state E_1 and different values of P_e, together with measurements at constant P_e as a function of the energy detuning of the excitation with respect to the E_1 maximum. This is shown in fig. 4, where a diagram of the energy levels and transitions is presented (a), together with the power dependence of Γ_R for resonant excitation (b) and the detuning dependence of Γ_R for constant excitation power (c), (d).

For resonant excitation (fig. 4(b)) one observes a linear increase of the antibunching rate with increasing pump power. In the low excitation limit ($P_e \to 0$) Γ_R tends to $2.1\,\mathrm{ns}^{-1}$, which is the Γ_X value measured by TRPL. This value is indicated by the open square in fig. 4(b). When the excitation energy is detuned from the excited state, a broadening of the antibunching dip is observed (figs. 3(c) and (d)), indicating a variation in the SPE dynamics at constant P_e. A plot of Γ_R as a function of detuning in the $-0.5 < \delta < 0.6$ meV range is shown in fig. 4(c) for 470 nW (open squares) and 230 nW (full squares) excitation power. Both sets of measurements are plotted together in fig. 4(d) after subtracting Γ_X (which is only weakly power dependent, as shown in fig. 2(b)) and then normalizing to the excitation power. The line in fig. 4(d) is the PLE spectrum shown in the inset of fig. 1. The noticeable coincidence of the normalized Γ_R values with the PLE profile of E_1 in

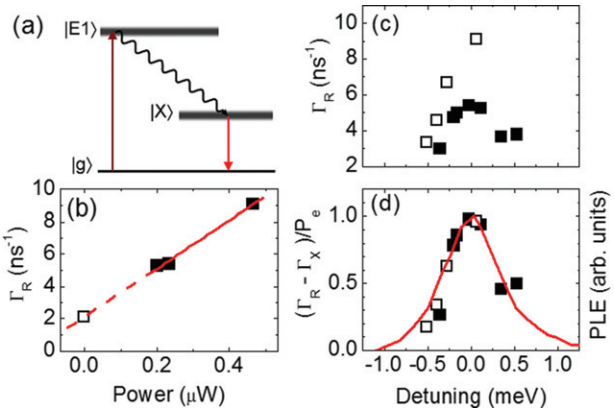

Fig. 4: (Color online) (a) Scheme of the energy levels in the QD. (b) Antibunching rate *vs.* excitation power at fixed $\delta = 0$ detuning (black squares). In the zero power limit Γ_R tends to $\Gamma_X = 2.1\,\mathrm{ns}^{-1}$ as measured by TRPL (open square). (c) Γ_R *vs.* detuning under quasi-resonant excitation at E_1 for 470 nW (open squares) and 230 nW (full squares) excitation power. (d) Same data as in (c) after subtraction of Γ_X and normalization to the excitation power. The line is the measured PLE spectrum plotted in the inset of fig. 1.

fig. 4(d) clearly indicates that the energy dependence of Γ_R is due to the absorption-induced variation of the pump rate γ. In other words, intra-dot excitation increases the occupation probability of X for decreasing δ in the same way as for increasing excitation power. A similar increase of Γ_R was observed in a QD coupled to a micro-cavity when the X state was brought into resonance with the cavity mode [27]. However, in that case the spontaneous exciton decay rate was enhanced by the Purcell effect, and the increase in Γ_R was due to the increase of Γ_X instead of to an increase of γ in eq. (4).

The phenomenon of photon bunching under intra-dot excitation, also observed in figs. 3(a), (b), sometimes named as "memory effect", has been explained by the "blinking" of single QDs [10,19,30]. It is due to the random change of the QD between "bright" and "dark" states, so photons tend to bunch during the bright periods [31,32] causing positive correlation. The blinking periods correspond then to the bunching times. In our case the "bright" and "dark" states are naturally assigned to the bright and dark states of the neutral exciton. Charged *vs.* neutral exciton states are not likely to be at the origin of the observed bunching [31] as CX is very weak under intra-dot excitation. The bunching rates Γ_B are approximately 50 times smaller than the antibunching ones. Contrary to the case of Γ_R, the Γ_B dependence on δ is not clear due to relatively large experimental noise.

In summary, the dynamics of the optical response of an InP/GaInP QD has been studied by optical spectroscopy including photon correlation under intra-dot excitation at the QD *p*-shell state for different values of energy detuning and excitation power. At constant excitation power the antibunching rate Γ_R increases as the pump rate for

resonant excitation ($|\delta| \to 0$). The spectral dependence of Γ_R is maintained for different excitation powers, as the exciton decay rate remains essentially unchanged. The presence of bunching is explained by the QD "blinking" originated by random changes between bright and dark exciton states.

* * *

This work was supported by the Spanish MINECO under contracts MAT2011-22997 and TEC2011-29120, by CAM under contract S2009/ESP-1503 and by the FP7 ITN Spin-optronics (237252). The authors are indebted with C. Tejedor for helpful discussions.

REFERENCES

[1] Kimble H. J., Dagenais M. and Mandel L., *Phys. Rev. Lett.*, **39** (1977) 691.
[2] Diedrich F. and Walther H., *Phys. Rev. Lett.*, **58** (1987) 203.
[3] De Martini F., Di Giuseppe G. and Marrocco M., *Phys. Rev. Lett.*, **76** (1996) 900.
[4] Lounis B. and Moerner W. E., *Nature*, **407** (2000) 491.
[5] Brouri R., Beveratos A., Poizat J.-P. and Grangier P., *Phys. Rev. A*, **62** (2000) 063817.
[6] Aharonovich I., Castelletto S., Simpson D. A., Greentree A. D. and Prawer S., *Phys. Rev. A*, **81** (2010) 043813.
[7] Michler P., Imamoğlu A., Mason M. D., Carson P. J., Strouse G. F. and Buratto S. K., *Nature*, **406** (2000) 968.
[8] Zwiller V., Aichele T. and Benson O., *Phys. Rev. B*, **69** (2004) 165307.
[9] Santori C., Fattal D., Vuckovic J., Solomon G. S. and Yamamoto Y., *Nature*, **419** (2002) 594.
[10] He Yu-Ming, He Yu, Wei Yu-Jia, Wu Dian, Atatüre M., Schneider C., Höfling S., Kamp M., Lu Chao-Yang and Pan Jian-Wei, *Nat. Nanotechnol.*, **8** (2013) 213.
[11] Malko A., Baier M. H., Karlsson K. F., Pelucchi E., Oberli D. Y. and Kapon E., *Appl. Phys. Lett.*, **88** (2006) 081905.
[12] Gazzano O., Michaelis de Vasconcellos S., Arnold C., Nowak A., Galopin E., Sagnes I., Lanco L., Lemaître A. and Senellart P., *Nat. Commun.*, **4** (2013) 1425.
[13] Reischle M., Beirne G. J., Rossbach R., Jetter M. and Michler P., *Phys. Rev. Lett.*, **101** (2008) 146402.
[14] Nowak A. K., Gallardo E., Sarkar D., van der Meulen H. P., Calleja J. M., Ripalda J. M., González L. and González Y., *Phys. Rev. B*, **80** (2009) 161305(R).
[15] Luxmoore I. J., Ahmadi E. D., Wasley N. A., Fox A. M., Tartakovskii A. I., Krysa A. B. and Skolnick M. S., *Appl. Phys. Lett.*, **97** (2010) 181104.
[16] Aichele T., Scholz M. and Benson O., *Proc. IEEE*, **95** (2007) 1791.
[17] Rossbach R., Reischle M., Beirne G. J., Jetter M. and Michler P., *Appl. Phys. Lett.*, **92** (2008) 071105.
[18] Hargart F., Kessler C. A., Schwarzbck T., Koroknay E., Weidenfeld S., Jetter M. and Michler P., *Appl. Phys. Lett.*, **102** (2013) 011126.
[19] Santori C., Pelton M., Solomon G., Dale Y. and Yamamoto Y., *Phys. Rev. Lett.*, **86** (2001) 1502.
[20] Santori C., Fattal D., Vučković J., Solomon G. S., Waks E. and Yamamoto Y., *Phys. Rev. B*, **69** (2004) 205324.
[21] Hanbury Brown R. and Twiss R. Q., *Nature*, **178** (1956) 1447.
[22] Mlinar V. and Zunger A., *Phys. Rev. B*, **80** (2009) 205311.
[23] Bacher G., Weigand R., Seufert J., Kulakovskii V. D., Gippius N. A. and Forchel A., *Phys. Rev. Lett.*, **83** (1999) 4417.
[24] Johansen J., Julsgaard B., Stobbe S., Hvam J. M. and Lodahl P., *Phys. Rev. B*, **81** (2010) 081304R.
[25] Martín M. D., Antón C., Viña L., Pietka B. and Potemski M., *EPL*, **100** (2012) 67006.
[26] Wimmer M., Nair S. V. and Shumway J., *Phys. Rev. B*, **73** (2006) 165305.
[27] Maragkou M., Nowak A. K., Gallardo E., van der Meulen H. P., Prieto I., Martinez L. J., Postigo P. A. and Calleja J. M., *Phys. Rev. B*, **86** (2012) 085316.
[28] Reischle M., Beirne G. J., Schulz W.-M., Eichfelder M., Rossbach R., Jetter M. and Michler P., *Opt. Express*, **16** (2008) 12771.
[29] Becher C., Kiraz A., Michler P., Imamoğlu A., Schoenfeld W. V., Petroff P. M., Zhang Lidong and Hu E., *Phys. Rev. B*, **63** (2001) 121312(R).
[30] Zinoni C., Alloing B., Li L. H., Marsili F., Fiore A., Lunghi L., Gerardino A., Vakhtomin Yu. B., Smirnov K. V. and Goltsman G. N., *Appl. Phys. Lett.*, **91** (2007) 031106.
[31] Bernard J., Fleury L., Talon H. and Orrit M., *J. Chem. Phys.*, **98** (1993) 2.
[32] Sallen G., Tribu A., Aichele T., Andr R., Besombes L., Bougerol C., Tatarenko S., Kheng K. and Poizat J. Ph., *Phys. Rev. B*, **80** (2009) 085310.